

## The critical current density of grain boundary channels in polycrystalline HTS and LTS superconductors in magnetic fields

This article has been downloaded from IOPscience. Please scroll down to see the full text article.

2013 Supercond. Sci. Technol. 26 095006

(<http://iopscience.iop.org/0953-2048/26/9/095006>)

View [the table of contents for this issue](#), or go to the [journal homepage](#) for more

Download details:

IP Address: 129.234.189.104

The article was downloaded on 14/08/2013 at 15:17

Please note that [terms and conditions apply](#).

# The critical current density of grain boundary channels in polycrystalline HTS and LTS superconductors in magnetic fields

P Sunwong, J S Higgins, Y Tsui, M J Raine and D P Hampshire

Department of Physics, Superconductivity Group, Centre for Materials Physics, University of Durham, South Road, Durham DH1 3LE, UK

E-mail: [d.p.hampshire@durham.ac.uk](mailto:d.p.hampshire@durham.ac.uk)

Received 17 April 2013, in final form 21 June 2013

Published 29 July 2013

Online at [stacks.iop.org/SUST/26/095006](http://stacks.iop.org/SUST/26/095006)

## Abstract

We provide evidence that a single mechanism—flux flow along channels—can explain the functional form of the critical current density ( $J_c$ ) in the low-temperature superconductor Nb<sub>3</sub>Sn and in the high-temperature superconductors (HTS) YBa<sub>2</sub>Cu<sub>3</sub>O<sub>7- $\delta$</sub>  (YBCO) and (Bi, Pb)<sub>2</sub>Sr<sub>2</sub>Ca <sub>$n-1$</sub> Cu <sub>$n$</sub> O <sub>$x$</sub>  (BiSCCO) in low and high magnetic fields. In this paper, we show that standard flux pinning theories, used for the past four decades to describe  $J_c$  in low-temperature superconductors (LTS), cannot explain the strain dependence of  $J_c$  in YBCO because  $J_c$  is a function of strain but the average superconducting properties are not. We conclude that in the polycrystalline samples presented here, the channels are grain boundaries that are narrow and metallic in Nb<sub>3</sub>Sn and YBCO but wide and semiconducting in BiSCCO. In Nb<sub>3</sub>Sn, strain alters  $J_c$  by changing the superconducting properties of the grains, whereas in YBCO, strain alters  $J_c$  by changing the properties of the grain boundaries.

(Some figures may appear in colour only in the online journal)

## 1. Introduction

A description of the long-standing approach used to increase the critical current density ( $J_c$ ) of polycrystalline low-temperature superconductors (LTS) such as Nb<sub>3</sub>Sn [1] in high magnetic fields, is probably best encapsulated by the flux pinning scaling laws used to parameterize the volume pinning force  $F_p$  and  $J_c$  given by [1, 2]

$$F_p = J_c B = \frac{\alpha}{D} B_{c2}^n \left( \frac{B}{B_{c2}} \right)^p \left( 1 - \frac{B}{B_{c2}} \right)^q, \quad (1)$$

where  $\alpha$ ,  $n$ ,  $p$  and  $q$  are constants,  $D$  is the grain size,  $B$  is the applied field and  $B_{c2}$  is the upper critical field. For Nb<sub>3</sub>Sn, this functional form best fits the data in fields above 1 or 2 T. The intrinsic properties of materials have been improved by doping to increase  $B_{c2}$  [3]. The extrinsic properties have been improved by reducing the grain size

to increase the density of grain boundaries; by adding precipitates, which increases the pinning and hence  $J_c$ ; and by changing the pinning mechanism operating to optimize  $p$  and  $q$  [4]. These approaches have successfully provided materials that enable applications from body scanners to the Large Hadron Collider [5]. However, the discovery of the weak-link problem in high-temperature superconductors (HTS) [6], including the exponential decay of  $J_c$  in high fields, suggested that transmission of supercurrent through the grain boundaries limits  $J_c$  in HTS such as YBa<sub>2</sub>Cu<sub>3</sub>O<sub>7- $\delta$</sub>  (YBCO) [7, 8]. This has meant that scientists developing HTS have adopted a different strategy to that used for LTS and focused on the formidable challenge of producing km-long quasi-single-crystalline materials with only (and as few as possible) low-angle grain boundaries [9]. In this paper we show that in the polycrystalline materials presented here, flux flow along grain boundaries can explain the functional form of

$J_c$  in both high and low fields in both LTS and HTS. Although it has long been known that flux flow along grain boundaries is a possible description of dissipation in polycrystalline superconductors, the many forces on the fluxons that operate in these materials and complex disorder in the flux-line-lattice have meant that until computational visualization of flux flow was obtained [10] (using time-dependent Ginzburg–Landau (TDGL) theory), there was no strong evidence that this is the dissipative state. Furthermore, there has been no mathematical framework to describe such dissipation. Recently, in our group, we have found analytic solutions that describe  $J_c$  for superconducting–normal–superconducting (SNS) junctions in high fields [11]. They are used here to model polycrystalline superconductors as a collection of such junctions. We present  $J_c$  measurements obtained as a function of field, temperature, angle of field and strain for (polycrystalline) Nb<sub>3</sub>Sn wire, YBCO tape and BiSCCO tape and show that a single mathematical framework describes the data.

## 2. Flux flow along grain boundaries

In low magnetic fields,  $J_c$  through a narrow SNS junction is given by the familiar sinc function [12, 13]

$$J_c = \frac{\hbar J^*(0)}{2ew(d + \lambda_{(S)})B} \left| \sin \frac{2ew(d + \lambda_{(S)})B}{\hbar} \right|, \quad (2)$$

where  $w$  is the width of the junction,  $(d + \lambda_{(S)})$  is known as the effective half-thickness of the junction and the penetration depth is  $\lambda_{(S)}$ . Since we consider anisotropic materials here, we distinguish parameters that are determined by the direction of current flow by a superscript star (associated with the effective mass of the carriers) from those determined by the angle of the applied field with respect to the crystallographic axes (e.g.  $B_{c2}^*$  and  $B_{c2}$ ). Equation (2) does not consider the complex spatial variation of the order parameter in the mixed state, where fluxon formation occurs in the junction and in the superconductor. TDGL computation in our group (on isotropic superconductors) has confirmed that for wide junctions or in high magnetic fields, where many fluxons are in the junction, the sine term, which is associated with the phase of the superelectrons, is averaged out to  $1/\sqrt{2}$  [11] (and we assume this averaged value remains correct for the highly textured HTS materials considered in this work). When the superconductor is in the mixed state and the magnetic field produces many fluxons in the junction, the factor  $(d + \lambda_{(S)})$  is replaced by  $(d + \xi_{(S)})$ . Complementary analytical work has led to a general solution for the depairing current  $J_{D-J}$  through one-dimensional SNS junctions [11] that accounts for the depression of the order parameter by the magnetic field and is given by

$$J_{D-J} = \frac{\rho_{(S)}}{\rho_{(N)}} \frac{B_{c2}^*}{\mu_0 \lambda_{(S)}^* \kappa^*} \hat{\psi}_\infty^2 \left( \frac{B}{B_{c2}} \right)^{\frac{1}{2}} \left( \frac{2B}{B_{c2}} \frac{d^2}{\xi_{(S)}^2} + \frac{1}{\gamma} \right)^{\frac{1}{2}} \times F^2 \exp \left( -\frac{B\gamma}{B_{c2}} \frac{d^2}{\xi_{(S)}^2} \right) \quad (3)$$

where

$$F = \left[ \sqrt{\left( \frac{\rho_{(S)}}{\sqrt{2}\rho_{(N)}} \frac{B\gamma}{B_{c2}} \frac{d}{\xi_{(S)}} \left( 1 - \frac{1}{\frac{2B\gamma}{B_{c2}} \frac{d^2}{\xi_{(S)}^2} + 1} \right) \right)^2 + 1} - \frac{\rho_{(S)}}{\sqrt{2}\rho_{(N)}} \frac{B\gamma}{B_{c2}} \frac{d}{\xi_{(S)}} \left( 1 - \frac{1}{\frac{2B\gamma}{B_{c2}} \frac{d^2}{\xi_{(S)}^2} + 1} \right) \right], \quad (4)$$

$\hat{\psi}_\infty^2 = (1-b)$ ,  $\gamma^2 = (1+eBd^2/\hbar)/(6+eBd^2/\hbar)$ ,  $\kappa = \lambda_{(S)}/\xi_{(S)}$  is the Ginzburg–Landau parameter and  $\rho_{(S)}$  and  $\rho_{(N)}$  are normal state resistivities of the superconducting grains and the normal grain boundaries respectively [14]. Note the form of  $\frac{B\gamma}{B_{c2}} \frac{d^2}{\xi_{(S)}^2}$  is used for convenience and does not strongly depend on the superconducting properties since it is equal to  $\frac{2eB\gamma d^2}{\hbar}$ .  $J^*(0)$  in (2) can then be equated to  $J_{D-J}$  of the junction, which gives:

$$J_c(B) \approx \frac{1}{\sqrt{2}} \frac{B_{c2}^*}{\mu_0 \xi_{(S)}^* (\kappa^*)^2} \frac{r \xi_{(S)}^2}{w(d + \xi_{(S)})} \left( \frac{1}{b} \right)^{\frac{1}{2}} \times \left( \frac{2bd^2}{\xi_{(S)}^2} + \frac{1}{\gamma} \right)^{\frac{1}{2}} F^2 (1-b) \exp \left( -\frac{b\gamma d^2}{\xi_{(S)}^2} \right) \quad (5)$$

where we have used dimensionless units  $r = \frac{\rho_{(S)}}{\rho_{(N)}}$  and  $b = \frac{B}{B_{c2}}$ . In high fields, we find experimentally (below) that  $d$  is equal to a few coherence lengths [15, 16], where

$$d = s[\xi_{(S)}(T) - d_0] \quad (6)$$

and  $s$  and  $d_0$  are constants. Our approach is phenomenological so the details of microscopic processes are neglected [17] and the parameters derived are assumed to be characteristic averages of the distributions of material properties that inevitably occur in inhomogeneous high- $J_c$  materials. We have not included the De Gennes [18] exponential term that characterizes the decay of the order parameter in zero field across a thick junction [11] because it is not required to fit the  $J_c$  data presented in this paper. The central proposition of this paper is that we can consider low-temperature and high-temperature polycrystalline superconductors as a collection of SNS junctions where equations (5) and (6) describe  $J_c$  in high and low magnetic fields, and where, above criticality, flux flows along grain boundary channels.

## 3. Samples and experimental techniques

Three different types of samples were measured: Multifilamentary DI-BiSCCO type HT tapes supplied by Sumitomo Electric Industries. The average width and thickness of the tapes were 4.5 mm and 0.36 mm, respectively; YBCO tapes from SuperPower (SCS4050). The superconducting layer was deposited onto a Hastelloy substrate with buffer layers, using a metal organic chemical vapour deposition technique, and stabilized by a copper layer. The superconducting YBCO layer was approximately 4 mm wide and 1  $\mu$ m

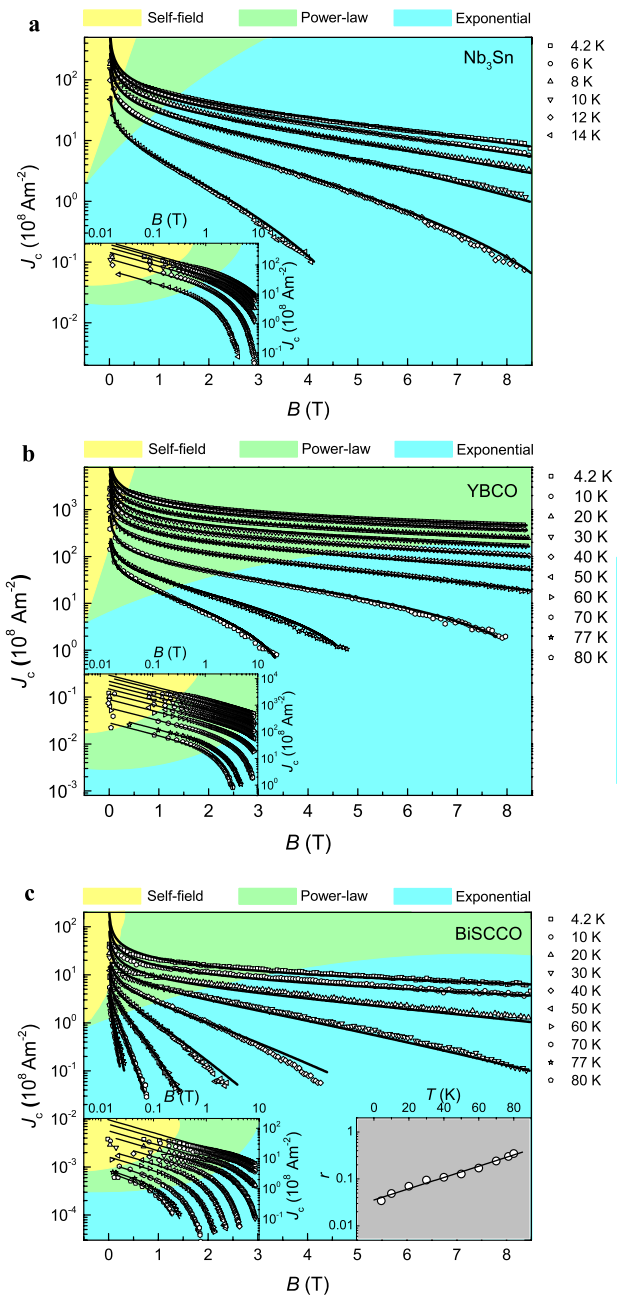
thick; Nb<sub>3</sub>Sn wires manufactured by Bruker EAS using the multifilamentary bronze-route process. The average diameter of the wires was 0.81 mm.

The magnetization  $J_c$  measurements and ac magnetic susceptibility measurements of YBCO, BiSCCO and Nb<sub>3</sub>Sn were completed in a Quantum Design Physical Properties Measurement System<sup>®</sup> in magnetic fields up to 8.5 T at different temperatures. In the magnetization measurements, hysteresis loops were obtained and the magnetization  $J_c$  was calculated using Bean's critical state model [19]. Ac magnetic susceptibility measurements were also used to find  $B_{c2}(T)$ .

The transport  $J_c$  measurements of Nb<sub>3</sub>Sn were made using a standard four-terminal technique and the critical currents were determined using a  $10 \mu\text{V m}^{-1}$  electric field criterion.  $J_c$  for YBCO and BiSCCO was determined at  $100 \mu\text{V m}^{-1}$ . The critical current densities were calculated using the critical current divided by the unstrained cross-sectional area of the superconducting components. Transport  $J_c$  measurements on Nb<sub>3</sub>Sn wires were performed at 4.2 K in magnetic fields up to 14.5 T in a vertical superconducting magnet using our purpose-built strain probe, which includes a copper beryllium spring sample holder [20, 21]. The measurements of YBCO and BiSCCO tapes were performed at 77 K in magnetic fields up to 0.7 T in a conventional iron-core electromagnet and at 4.2 K in magnetic fields up to 14 T in a 40-mm-bore horizontal split-pair superconducting magnet for different angles between the field and the tape surface. The strain measurements were carried out by using a springboard-shaped copper beryllium sample holder to apply strains up to 0.3% in tension and  $-1.3\%$  in compression [22, 23].

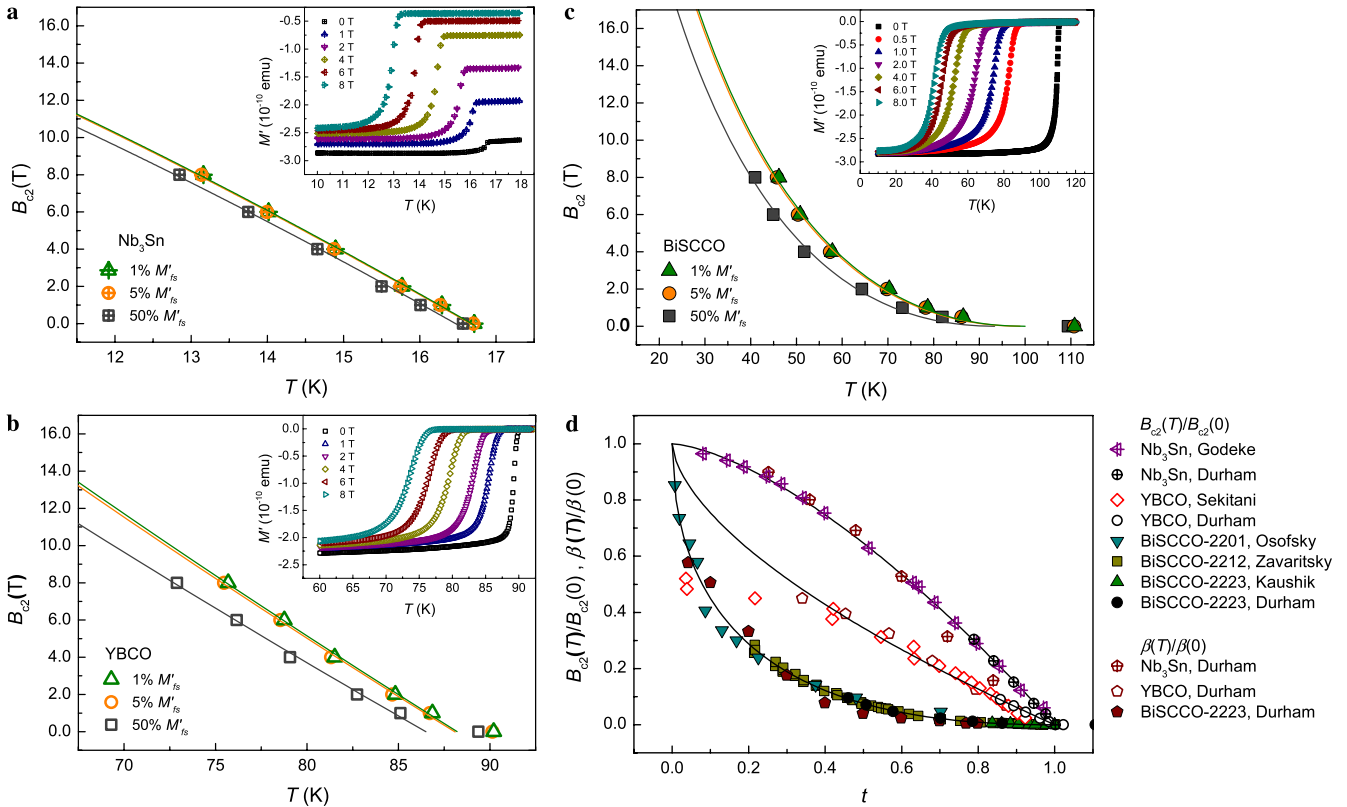
#### 4. Experimental functional form of $J_c$

Figure 1 shows magnetization  $J_c$  as a function of applied magnetic field and identifies what we call in this work the self-field regime, the power-law regime and the exponential regime. The solid lines are fits to the data using equations (5) and (6), where we have assumed that the Ginzburg–Landau constants are 33, 94 and 139 for Nb<sub>3</sub>Sn, YBCO and BiSCCO respectively [24]. At the very lowest fields, the (log–log) insets of figure 1 show that  $J_c$  is independent of field and the range over which  $J_c$  is field-independent decreases as the temperature increases. This is consistent with the self-field produced by the flowing current being much higher than the external magnetic field. At low fields,  $J_c(B)$  shows power-law behaviour with an exponent of  $-0.5$ , consistent with equation (5). The power-law behaviour occurs over a wider range of fields and temperatures for YBCO than for Nb<sub>3</sub>Sn and BiSCCO, and is attributed (below) to thinner grain boundaries. At sufficiently high fields, there is a cross-over from the power-law to the exponential regime, which has been observed experimentally by other authors [25–28]. We note that in other (lower  $J_c$ ) YBCO samples,  $J_c(B)$  is exponential over several orders of magnitude and a much larger range of field and temperature phase space [29] than shown here, which is consistent with attributing the field dependence to the nature of the grain boundaries and not the intrinsic properties of any specific superconducting material.



**Figure 1.** Three regimes of magnetic field dependence of the critical current density. (a) Log-linear plots of magnetization critical current density versus magnetic field calculated using Bean's critical state model [19] for a Nb<sub>3</sub>Sn wire, showing the self-field regime (yellow), power-law behaviour (green) and exponential behaviour (blue). The inset is a log–log plot of the same data, showing power-law behaviour in low fields. (b), (c) Similar plots for YBCO and BiSCCO for the field parallel to the  $c$ -axis of the tape. In (c), an additional inset shows the temperature dependence of  $r$ , consistent with semiconducting behaviour of the BiSCCO grain boundaries. Solid lines are fits to equations (5) and (6).

The functional form of  $B_{c2}(T)$  has been derived for each of the three materials studied here from fitting the  $J_c$  data to equations (5) and (6). In figure 2, we have compared these functional forms with  $B_{c2}$  values from the literature, as well as with those obtained from in-house ac magnetic



**Figure 2.** Temperature dependence of the upper critical magnetic field. (a) Upper critical field of  $Nb_3Sn$  versus temperature obtained from ac magnetic susceptibility measurements that are shown in the inset. The upper critical magnetic field is shown at 1%, 5% and 50% of full screening ( $M'_{fs}$ ). The solid lines are fits to the in-field data with  $B_{c2}(T) = B_{c2}(0)(1 - t^{1.5})$ , giving the values of  $B_{c2}(0)[T_c]$  of 26.3 T [16.7 K], 26.3 T [16.7 K] and 25.3 T [16.5 K]. (b) Equivalent YBCO data with the field applied along the  $c$ -axis of the tape. The solid lines are fits to the data with  $B_{c2}(T) = B_{c2}(0)(1 - t^{0.61})$ , giving the values of  $B_{c2}(0)[T_c]$  of 89.0 T [88.2 K], 88.2 T [88.1 K] and 79.6 T [86.5 K]. (c) Equivalent BiSCCO data, where the solid line fits are  $B_{c2}(T) = B_{c2}(0)(1 - t^{0.5})^{2.1}$ , with fitting parameters of 84.5 T [100.2 K], 83.7 T [99.7 K] and 74.4 T [93.7 K] respectively. (d) Normalized  $B_{c2}$  and  $\beta$  as a function of reduced temperature for  $Nb_3Sn$ , YBCO and BiSCCO. Durham's  $B_{c2}$  data are taken from (a)–(c) at 1%  $M'_{fs}$ . Durham's  $\beta$  data are taken from the magnetization critical current density in figure 1 fitted in the high-field regime.  $\beta(0)$  for  $Nb_3Sn$ , YBCO and BiSCCO are 6.8 T, 23.4 T and 13.5 T respectively. The lines describe the reduced temperature relations for  $B_{c2}(T)$  given in (a)–(c) that were obtained from fits to the  $J_c$  data, where  $B_{c2}(0)[T_c]$  are 26.3 T [16.2 K], 68.5 T [87.6 K] and 84.5 T [110.8 K] respectively. The data from the literature are from Godeke [33], Sekitani [34], Osofsky [35], Zavaritsky [36] and Kaushik [37].

susceptibility measurements.  $B_{c2}$  has been characterized at 1%, 5% and 50% of full screening  $M'_{fs}$  in order to quantify how sensitive the values are to the criterion used. For  $Nb_3Sn$  (one of the important superconducting materials used in the ITER tokamak [30]), there is an enormous amount of data in the literature on samples fabricated by different routes and with different microstructure.  $B_{c2}(T)$  obeys the Werthamer–Helfand–Hohenberg (WHH) equation and can be characterized by  $B_{c2}(T) = B_{c2}(0)(1 - t^{1.5})$ , where  $t = T/T_c$  is the reduced temperature [31–33]. The data at 1% of screening give values of  $B_{c2}(0)$  and  $T_c$  of 26.3 T and 16.7 K, which are similar to those derived from the  $J_c$  data ( $B_{c2}(0)$  and  $T_c$  are 26.3 T and 16.2 K) and the literature data. For HTS, the fundamental properties and their variation with sample preparation and microstructure are far less well known, particularly at low temperatures, where  $B_{c2}(T)$  values are high. Nevertheless for YBCO, pulsed-field  $B_{c2}(T)$  data available up to 400 T [34] are shown in figure 2(d). We have used  $B_{c2}(T) = B_{c2}(0)(1 - t^{0.61})$  to fit the  $J_c$  data with values of  $B_{c2}(0)$  and  $T_c$  of 68.5 T and

87.6 K, which only differ significantly from the pulsed-field temperature dependence at 25 K and below, where we find an upward curvature in  $B_{c2}$ . This curvature may arise from the difference in magnitude of  $B_{c2}(0)$  between the single-crystal sample used for pulsed-field measurements and our tape, optimized for high  $J_c$ , or our assumption that  $\kappa$  is independent of temperature. A concave curvature of  $B_{c2}(T)$  has been observed in several BiSCCO systems [35–37] which can be characterized using a scaling function  $B_{c2}(T) = B_{c2}(0)(1 - t^{0.5})^{2.1}$ , where fitting parameters from the  $J_c$  data for our BiSCCO sample are  $B_{c2}(0) = 84.5$  T and  $T_c = 110.8$  K. The data in figure 2 show that there is reasonably good agreement between the reduced temperature dependence and the free parameters obtained from different measurements on different samples. For BiSCCO, the current densities are a significantly smaller fraction of the depairing current density than, for example, in YBCO. When fitting the BiSCCO data at low fields, we find that unlike  $Nb_3Sn$  or YBCO, the temperature dependence for  $J_c$  cannot be explained by the temperature dependence of  $B_{c2}$  alone. We attribute the different behaviour

of BiSCCO to the temperature dependence of  $r$  and describe it empirically by  $r(T) = r_0 \exp(T/T_0)$ , where  $r_0 = 3.6 \times 10^{-2}$  and  $T_0 = 36$  K in the fits to the data. The temperature dependence of  $r$  is consistent with  $\rho_{(N)}$  (associated with the grain boundary) increasing with decreasing temperature. Also shown in figure 2 are values of  $\beta(T)$ . We found  $\beta(T)$  for all three materials by assuming that in the high-field regime, in fields not too close to  $B_{c2}(T)$ , we can simply consider  $J_c$  to be proportional to  $\exp[-B/\beta(T)]$ . For YBCO, we did not make measurements in sufficiently high magnetic fields to reach the high-field exponential regime at low temperatures. Nevertheless the data in figure 2 show the temperature dependence of  $\beta(T)$  is similar to  $B_{c2}(T)$  for all three materials (where comparison is available) and has led to the empirical equation (6).

The anisotropy of YBCO and BiSCCO can be described using anisotropic Ginzburg–Landau theory, which relates the angle  $\theta$  between the magnetic field and the  $a$ – $b$  plane of the crystal structure using  $B_{c2}(\theta) = B_{c2}(\pi/2)(\sin^2\theta + \Gamma^{-2} \cos^2\theta)^{-1/2}$  [38], where  $\Gamma$  characterizes the degree of anisotropy. Here we treat YBCO and BiSCCO as anisotropic layered superconductors with three-dimensional behaviour. Although weak Josephson coupling between superconducting layers in BiSCCO leads to two-dimensional behaviour at low temperature and is described most accurately using Lawrence–Doniach theory [39], the  $B_{c2}$  values calculated from these two theories are only significantly different at very low  $\theta$  and are almost indistinguishable for very highly anisotropic materials and the data considered here.

We have measured  $J_c$  as a function of field, strain and angle at 77 and 4.2 K in a standard vertical magnet (Nb<sub>3</sub>Sn) and a horizontal split-pair magnet (YBCO and BiSCCO) using dedicated probes designed in-house for transport measurements. Current flow is orthogonal to the field at all angles. These transport experiments are particularly demanding in the split-pair magnet at 4.2 K because of the large forces on the samples. However, the angular measurements have the advantage that, unlike angular magnetic measurements, the interpretation of the data is more straightforward because the path of the macroscopic current flow is unambiguous. In figure 3, the angular dependence of  $J_c$  is shown. Equation (5) implies that universal scaling behaviour should be observed for the angular dependence of  $J_c$  as a function of  $B(\sin^2\theta + \Gamma^{-2} \cos^2\theta)^{1/2}$ . This universality is confirmed as a function of angle at several magnetic fields for YBCO at 4.2 K and at three different strains as a function of field and angle for BiSCCO. We attribute the relatively small asymmetry about 0 degrees at 4.2 K (figure 3(b)) and at 77 K (not shown) for YBCO predominantly to angular hysteresis [40] and pinning (cf section 5). The values of the anisotropy constant  $\Gamma$  obtained for YBCO and BiSCCO are 7.0 and 7.8 respectively, which are both within the range of values quoted in the literature. The YBCO sample used in this work was fabricated by deposition of YBCO film onto substrates with relatively good crystallographic alignment (misalignment less than 10° FWHM) [41] consistent with literature values for the anisotropy constant of 3–8 [12, 42, 43].

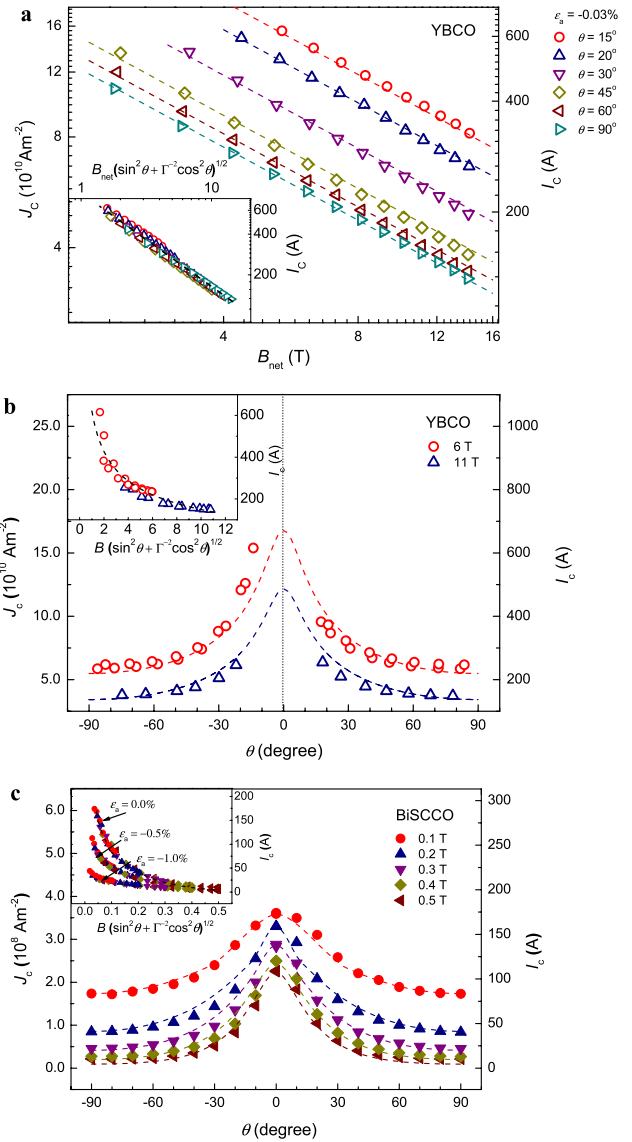


**Figure 3.** Anisotropic properties of YBCO and BiSCCO. (a) Transport critical current density of a YBCO tape at 4.2 K versus field for different angles between the magnetic field and the tape surface. Inset, data replotted as a universal curve versus  $B(\sin^2\theta + \Gamma^{-2} \cos^2\theta)^{1/2}$ , where  $\Gamma$  is 7.0. (b) Transport critical current density of YBCO at 4.2 K versus angle between the magnetic field and the tape surface at 6 and 11 T. Inset, data replotted as a universal curve, where  $\Gamma$  is 7.0. (c) Transport critical current density of BiSCCO tapes at 77 K versus angle between the magnetic field and the tape surface for zero applied strain. Inset, data replotted as a universal curve as well as data at two other strains, where  $\Gamma$  is 7.8. Dotted lines are guides to the eye.

For BiSCCO, the anisotropy is at the low end of the range reported in the literature ( $\Gamma = 3$ –150 [44–47]). We attribute the value of  $\Gamma$  predominantly to anisotropy, but it is also affected by grain misalignment, which is important in BiSCCO since the tape was produced by the powder-in-tube (PIT) method. In both tapes the  $c$ -axis is preferentially orthogonal to the surface of the tape.

Figure 4 shows the normalized critical current density  $J_n$  (where  $J_n = J_c(\epsilon_a)/J_c(\epsilon_p)$ ) versus strain. Relative strain ( $\epsilon_r$ ) is defined by:  $\epsilon_r = \epsilon_a - \epsilon_p$ , where  $\epsilon_a$  is the applied strain and

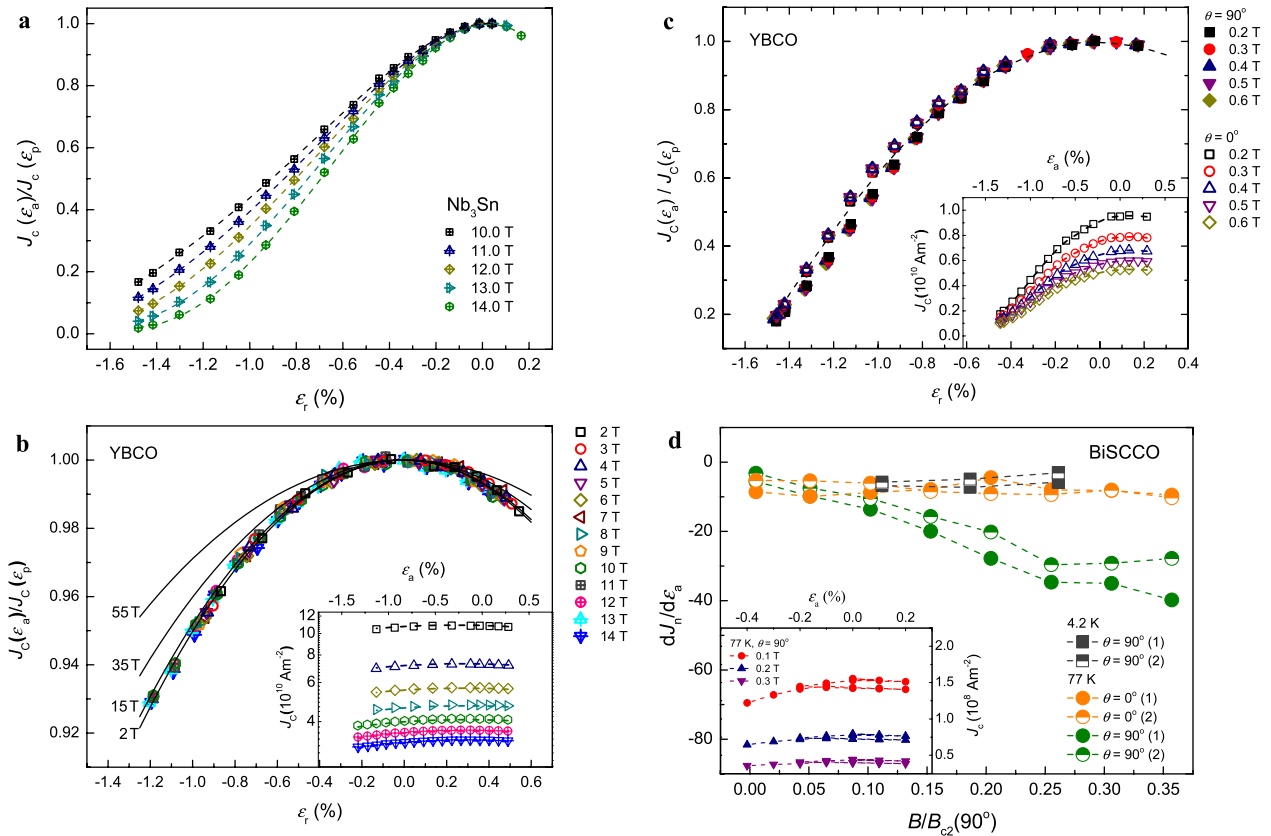


**Figure 4.** Effect of strain on the critical current density. (a) Normalized critical current density,  $J_n = J_c(\epsilon_a)/J_c(\epsilon_p)$  of a Nb<sub>3</sub>Sn wire versus relative strain at 4.2 K for different applied magnetic fields. (b) Current density of a YBCO tape versus applied strain (inset). Normalized critical current density of YBCO versus relative strain at 4.2 K at different magnetic fields applied parallel to the  $c$ -axis.  $J_n(\epsilon)$  shows power-law magnetic field behaviour and  $\epsilon_p$  is a weak function of field. Also shown as solid lines are calculations of  $J_c$  at very high fields. (c) Critical current density of a YBCO tape versus applied strain at 77 K for different fields applied parallel and orthogonal to the  $c$ -axis.  $J_n$  of YBCO versus relative strain at 77 K at different magnetic fields applied parallel and orthogonal to the  $c$ -axis. (d)  $J_c$  versus strain for a BiSCCO tape (inset).  $dJ_n/d\epsilon_a$  as a function of reduced magnetic field for the  $B \parallel c$ -axis orientation ( $B/B_{c2}(90^\circ)$ ) for BiSCCO at 4.2 and 77 K for two different orientations of magnetic field. Only reversible  $J_c$  data were used to obtain  $dJ_n/d\epsilon_a$ . Labels (1) and (2) represent the first and the second reversible lines as seen in the inset. Dotted lines are guides to the eye.

$\epsilon_p$  is the value of strain at which  $J_c$  reaches its peak value. For Nb<sub>3</sub>Sn, there is the very strong field dependence expected for the strain dependence of  $J_n$  over the reduced field  $B/B_{c2}$  range 0.3–0.5. The strong effect of strain on the critical current density in LTS is attributed to the strong strain dependence of the superconducting properties  $B_{c2}$  and  $T_c$  and has been established for many Nb<sub>3</sub>Sn samples in the literature [48].

For YBCO,  $J_c$  is shown for both  $B$  parallel and orthogonal to the  $c$ -axis of the samples at 77 K as a function of strain. At 4.2 K, measurements as a function of strain were only made with  $B$  oriented parallel to the  $c$ -axis to keep currents below 500 A. The strain at which the maximum value of  $J_c(\epsilon_p)$  occurred, changed from  $-0.3\%$  at 2 T to  $-0.1\%$  at 14 T, as has been reported before [49] (although we saw no such change at 77 K, nor did we see the double-peak in  $J_c$  versus strain observed elsewhere [49, 50]). We attribute these changes to the field and strain dependence of the normal state properties of the grain boundaries. Unlike Nb<sub>3</sub>Sn, the normalized  $J_c$  for YBCO is an almost universal function of relative strain, independent of magnetic field over a large range of  $B/B_{c2}$  from  $\sim 0.06$  to 0.4 at 4.2 K, and both field and angle at 77 K. These results mean that  $B_{c2}$  and  $s$  are unaffected by strain (and

from WHH theory [31]  $\rho(s)$  also) at these temperatures. At 77 K, the anisotropy constant  $\Gamma$  (characterized over a range of  $70^\circ$ ) is also confirmed to be independent of strain for YBCO (figure 4(c)) and BiSCCO (inset to figure 3(c)). We conclude that the strain dependence of  $J_c$  is due to the strain dependence of  $r$ , and hence  $\rho(N)$ . Measurements of  $\rho(N)$  are required to explain why the strain dependence of  $r$  is larger at 77 K than at 4.2 K and may require inclusion of the role of grain boundary dislocations as a function of strain [51]. We note that since flux pinning theories do not include normal state properties, they cannot explain the variable-strain  $J_c$  data presented here in figures 4(b) and (c) for YBCO at all. Given the data show that  $B_{c2}$  is unaffected by strain, if one used a flux pinning description given by equation (1), a parameterization of the variable-strain  $J_c$  data would require a change in the grain size by a factor of five at 77 K, which is clearly not physical. In figure 4(b), we show how the strain-dependent  $r$  eventually causes the universal behaviour to break down (in the high-field exponential regime) and leads to a less strain-dependent normalized  $J_c$  on approaching  $B_{c2}$ . Since  $B_{c2}$  is independent of strain at both 4.2 and 77 K, we can expect that  $T_c$  is also independent of strain. Because  $J_c$

is a complex parameter, determined by a range of different local properties, including anisotropy, grain orientation, local defects and compositional properties, and grain boundary structures, the fitting parameters derived here are sample averaged and one can expect percolative current flow in a twinned YBCO tape. Single-crystal data on YBCO show that  $T_c$  increases with pressure along the  $b$ -axis and decreases with pressure along the  $a$ -axis, with an average that is close to being independent of strain [52]. Hence the single-crystal data on YBCO suggest that although the average superconducting properties are independent of strain, the underlying width of the distribution of the properties may change.

For BiSCCO, we found that accurate measurements of the strain dependence of  $J_c$  are demanding because the changes in  $J_c$  over the range of strain where  $J_c$  is reversible are much smaller than found in YBCO or  $\text{Nb}_3\text{Sn}$ . In the inset to figure 4(d), we show the ‘roof-top’ behaviour for  $J_c$  versus strain, which we have characterized in the reversible strain region using the change in the normalized  $J_c$  with strain (at zero applied strain) as a function of reduced field  $B/B_{c2}(90^\circ)$ . For  $B \parallel a$ - $b$  at 77 K and  $B \parallel c$ -axis at 4.2 K, data are only available over a limited range of reduced field,  $J_c$  is in the power-law regime and we find  $dJ_n/d\varepsilon_a$  is almost independent of magnetic field. As with the YBCO data, this suggests that, at least in this orientation,  $B_{c2}$  and  $s$  are unaffected by strain. However, for  $B \parallel c$  at 77 K,  $J_c$  is in the exponential regime and  $dJ_n/d\varepsilon_a$  is increasingly sensitive to strain as the applied field increases. This increase cannot be explained by a strain dependence of  $r$  because it causes a decrease in strain sensitivity in high fields. However, an increase of just 5% in  $d$  for a tensile strain of 1% explains the increasing strain sensitivity shown by the 77 K,  $B \parallel c$ -axis data in figure 4(d). Nevertheless without data at much higher fields we cannot determine whether this is due to changes in  $B_{c2}$  (which has been observed [53]) or  $s$ .

The  $r$  parameter (shown in table 1) is unity and independent of temperature for both  $\text{Nb}_3\text{Sn}$  and YBCO. These results imply that the resistivity of the grain boundaries and the grains in these materials have a similar temperature dependence and so are both metallic. For BiSCCO,  $r$  is small, with a temperature dependence consistent with the grain boundaries being highly resistive and semiconducting. Although the ratio  $r/w$  is fixed when parameterizing the BiSCCO  $J_c$  data, because the parameter  $w$  is strongly correlated with  $r$  and so can change without significant changes in the quality of fit, we have provided fits to the data with  $w$  set equal to that of YBCO. The presence of the parameter  $w$  in equation (5) explains why decreasing grain size was so effective in LTS materials and flux pinning theory has been so useful, since (using the language of pinning) the edges of the junctions can be interpreted as pinning sites. Since  $w$  is a few microns in  $\text{Nb}_3\text{Sn}$ , about a factor of 5–10 larger than the grain size [54], it suggests that several grains act together as a single channel, or equivalently not all triple points separate the channels (probably because they are not aligned sufficiently with the field direction). The HTS YBCO and BiSCCO have much smaller values of  $w$  than the grain sizes in these

**Table 1.** The parameters  $r(T = 0)$ ,  $w$ ,  $s$ ,  $T_c$  and  $d_0$  for  $\text{Nb}_3\text{Sn}$ , YBCO and BiSCCO fitted to the  $J_c$  data using equations (5) and (6).

	$r(T = 0)$	$w$	$s$	$T_c$ (K)	$d_0$
$\text{Nb}_3\text{Sn}$	1.0	4.2 $\mu\text{m}$	1.9	16.2	0
YBCO	1.0	122 nm	1.2	87.6	0
BiSCCO	$3.6 \times 10^{-2}$	122 nm	6.0	110.8	2.0 nm

materials [55–57], which implies that faceting or grain boundary dislocations divide a grain boundary into many SNS junctions, or to use the language of flux pinning, there are strong pinning sites along the grain boundaries [41, 58, 59]. In parameterizing the free-parameter  $d$ , we need only introduce the constant  $d_0$  to describe the BiSCCO  $J_c$  data, and even in this case  $d_0$  is sufficiently small that it only significantly affects  $d$  at the very lowest temperatures, where the fundamental superconducting properties are least well known. Simple arguments can provide an explanation for the values of  $s$  found:  $s$  is small in YBCO because  $B_{c2}$  is not dependent on strain and the low-angle grain boundaries are thin;  $s$  is larger in  $\text{Nb}_3\text{Sn}$  because the mechanism that causes superconductivity is different in LTS from HTS so, unlike YBCO, strain depresses the superconductivity near the grain boundaries [32]; and  $s$  is largest in BiSCCO because the PIT route produces relatively large-angle grain boundaries. Detailed compositional, structural and electronic information near the grain boundaries will be necessary to provide a more detailed explanation for the  $s$  values measured here.

## 5. Channels and artificial pinning in superconductors

This work shows that channels are an essential component of a proper description of  $J_c$  in polycrystalline superconductors. The mathematical framework described, helps to characterize local grain boundary properties from  $J_c$  measurements, unifies our understanding of  $J_c$  in LTS and HTS and informs new grain boundary engineering strategies for improving  $J_c$  in both LTS and HTS. For polycrystalline materials, equations (5) and (6) most obviously describe channels formed by grain boundaries. Long-standing literature developed to explain the field dependence of  $J_c$  in HTS materials proposes two different mechanisms to separately explain the power-law dependence by pinning and the exponential dependence by thermally activated pinning (i.e. flux creep) of vortices in the bulk [60, 61]. However, these historical models are flux pinning models which cannot describe the strain dependence of  $J_c$  in YBCO reported here. This paper uses a single functional form that naturally leads to power-law behaviour at low field and exponential behaviour in high fields without introducing two mechanisms. Although the model presented here described by equations (5) and (6) seems to be mathematically more daunting than the flux pinning equation given in equation (1), the number of free parameters is not significantly different. Comparing (1) with (5) and (6), the parameters  $n$ ,  $p$  and  $q$  in (1) are effectively replaced by  $s$  and the parameters  $\alpha$  and  $D$  by  $w$ . If the results  $d_0 = 0$  and  $r = 1$  found here for  $\text{Nb}_3\text{Sn}$  and YBCO are generally true for

metallic superconductors with well-connected grains, there is actually a reduction in the number of parameters required to specify the functional form of  $J_c$ . This reduction will help magnet engineers assess the merits of the many different superconducting materials available for applications.

Significant improvements in YBCO [62] and BiSCCO [63] have been achieved by heavily loading these materials with artificial pinning (AP). In YBCO, ion irradiation [62] and nanodots [64] have been successful. More recently, self-assembling nano-columns aligned along the  $c$ -axis of the material have also been very effective in increasing  $J_c$  by helping to reduce the angular variation (i.e. anisotropy) in  $J_c$  as a function of the direction of the applied field [65, 66]. In this context, it is helpful to consider a range of different microstructures determining  $J_c$ , from those materials with isolated pinning sites, those with pinning sites joined by shallow channels and those with joined-up deep channels alone. Even in high- $J_c$  quasi-single-crystal thin films with large low-angle (non-planar) grain boundaries, we can expect that when the density of dislocations is sufficiently high, some (small) parts of the film consist of channels made up of chains of dislocations. Until we know the mechanism that causes superconductivity, it is difficult to know the spatial extent of the disruption in superconductivity near a dislocation (for example, from local changes in the electronic band-structure or composition) or what maximum dislocation separation retains overlap and provide channels for flux flow. Indeed, this lack of knowledge hinders us more generally from relating the structure and composition of superconducting materials (i.e. electron microscopy data) to their transport properties (i.e.  $J_c$  data). The power-law/exponential field dependence of  $J_c$  found, for example, in some high dislocation density single-crystal thin films (with few grain boundaries) of YBCO [60, 67, 68] or some very high  $J_c$  BiSCCO [61] materials, provides evidence that flux flows along channels. We suggest that in order to parameterize  $J_c(B, T, \varepsilon, \theta)$  comprehensively in such materials with pinning and channels, one may usefully introduce an anisotropy in (or angular dependence to) the width ( $w$ ) of the channels that competes with the intrinsic anisotropy of the HTS material itself. Whether AP is practical for improving LTS polycrystalline materials is still an open question, but increasingly we can expect state-of-the-art HTS materials to have both channels and multiple types of AP operating [69]. In future there will be the real challenges of identifying what multiple processes are limiting  $J_c$  in such complex materials and how to parameterize  $J_c$ .

## 6. Concluding comments

Flux pinning theory can provide important insights into how  $J_c$  arises and is particularly useful if the pinning sites are well separated and the number of fluxons is very small. However, it cannot describe the strain dependence of  $J_c$  in YBCO reported here. Historically, the isotope effect led to an understanding of the phonon-mediated fundamental mechanism in LTS superconductors and phonons provided an explanation for the strain dependence of  $B_{c2}$  in the LTS Nb<sub>3</sub>Sn [48]. The evidence that strain does not affect

the average superconducting properties of YBCO may yet provide an important insight into the mechanism that gives rise to superconductivity in HTS [70, 71].

## Acknowledgments

We are grateful to Professor Osamura (RIAS) and Drs Sato and Fujikami (Sumitomo Electric Industries Ltd) for providing the multifilamentary DI-BiSCCO type HT tapes and acknowledge important discussions with them. This work was supported by EPSRC (Grant: EP/C535758/1) and a Royal Government of Thailand (DPST) PhD Scholarship.

## References

- [1] Schauer W and Schelb W 1981 Improvement of Nb<sub>3</sub>Sn high field critical current by a two-stage reaction *IEEE Trans. Magn.* **17** 374–7
- [2] Dew-Hughes D 1974 Flux pinning mechanisms in type II superconductors *Phil. Mag.* **30** 293–305
- [3] Flukiger R *et al* 2008 Optimization of Nb<sub>3</sub>Sn and MgB<sub>2</sub> wires *Supercond. Sci. Technol.* **21** 054015
- [4] Bonney L A, Willis T C and Larbalestier D C 1995 Dependence of critical current density on microstructure in the SnMo<sub>6</sub>S<sub>8</sub> Chevrel-phase superconductor *J. Appl. Phys.* **77** 6377–87
- [5] Rossi L 2010 Superconductivity: its role, its success and its setbacks in the Large Hadron Collider of CERN *Supercond. Sci. Technol.* **23** 034001
- [6] Dimos D, Chaudhari P, Mannhart J and LeGoues F K 1988 Orientation dependence of grain-boundary critical currents in YBa<sub>2</sub>Cu<sub>3</sub>O<sub>7- $\delta$</sub>  bicrystals *Phys. Rev. Lett.* **61** 219–22
- [7] Hilgenkamp H and Mannhart J 2002 Grain boundaries in high- $T_c$  superconductors *Rev. Mod. Phys.* **74** 485–549
- [8] Hsiang T Y and Finnemore D K 1980 Superconducting critical currents for thick, clean superconductor–normal-metal–superconductor junctions *Phys. Rev. B* **22** 154–63
- [9] Larbalestier D C *et al* 1988 Weak links and the poor transport critical currents of the 123 compounds *Physica C* **153–155** 1580–5
- [10] Carty G and Hampshire D P 2008 Visualising the mechanism that determines the critical current density in polycrystalline superconductors using time-dependent Ginzburg–Landau theory *Phys. Rev. B* **77** 172501
- [11] Carty G J and Hampshire D P 2013 The critical current density of an SNS junction in high magnetic fields *Supercond. Sci. Technol.* **26** 065007
- [12] Tinkham M 1996 *Introduction to Superconductivity* 2nd edn (Singapore: McGraw-Hill)
- [13] Poole C P, Farach H A and Creswick R J 1995 *Superconductivity* (San Diego, CA: Academic)
- [14] Schmid A 1966 A time dependent Ginzburg–Landau equation and its application to the problem of resistivity in the mixed state *Phys. Kondens. Mater.* **5** 302–17
- [15] Nikulov A V and Remisov Y D 1991 The critical current of the Josephson junction with boundaries in the mixed state: application to HTSC polycrystalline materials *Supercond. Sci. Technol.* **3** 312–7
- [16] Barone A and Paterno G 1982 *Physics and Applications of the Josephson Effect* (New York: Wiley)
- [17] Castro H *et al* 2008 Tunneling spectroscopy: a probe for high- $T_c$  superconductivity *Microelectron. J.* **39** 1296–9
- [18] De Gennes P G 1989 *Superconductivity of Metals and Alloys* (Redwood City, CA: Addison-Wesley)
- [19] Bean C P 1964 Magnetization of high-field superconductors *Rev. Mod. Phys.* **36** 31–9

- [20] Walters C R, Davidson I M and Tuck G E 1986 Long sample high sensitivity critical current measurements under strain *Cryogenics* **26** 406–12
- [21] Cheggour N and Hampshire D P 2000 A probe for investigating the effects of temperature, strain, and magnetic field on transport critical currents in superconducting wires and tapes *Rev. Sci. Instrum.* **71** 4521–30
- [22] Sunwong P, Higgins J S and Hampshire D P 2011 Angular, temperature and strain dependencies of the critical current of DI-BSCCO tapes in high magnetic fields *IEEE Trans. Appl. Supercond.* **21** 2840–4
- [23] Higgins J S and Hampshire D P 2011 Critical current density of  $\text{YBa}_2\text{Cu}_3\text{O}_{7-\delta}$  coated conductors under high compression in high fields *IEEE Trans. Appl. Supercond.* **21** 3234–7
- [24] Hampshire D P 1998 A barrier to increasing the critical current density of bulk untextured polycrystalline superconductors in high magnetic fields *Physica C* **296** 153–66
- [25] Bulaevskii L N, Daemen L L, Maley M P and Coulter J Y 1993 Limits to the critical current in high- $T_c$  superconducting tapes *Phys. Rev. B* **48** 798
- [26] Le Lay L, Friend C M, Maruyama T, Osamura K and Hampshire D P 1994 Evidence that pair breaking at the grain boundaries of  $\text{Bi}_2\text{Sr}_2\text{Ca}_2\text{Cu}_3\text{O}_x$  tapes determines the critical current density above 10 K in high fields *J. Phys.: Condens Matter* **6** 10053–66
- [27] Mawatari Y, Yamasaki H, Kosaka S and Umeda M 1995 Critical current properties and vortex-glass-liquid-transition in Ag-sheathed Bi-2223 tapes *Cryogenics* **35** 161–7
- [28] Dhalle M *et al* 1997 Experimental assesment of the current-limiting mechanisms in BSCCO/Ag high temperature superconducting tapes *Supercond. Sci. Technol.* **10** 21–31
- [29] Hampshire D P and Chan S-W 1992 The critical current density in high fields in epitaxial thin films of  $\text{YBa}_2\text{Cu}_3\text{O}_7$ : flux pinning and pair-breaking *J. Appl. Phys.* **72** 4220–6
- [30] Aymar R 2001 ITER R&D: executive summary: design overview *Fusion Eng. Des.* **55** 107–18
- [31] Werthamer N R, Helfand E and Hohenberg P C 1966 Temperature and purity dependence of the superconducting critical field,  $H_{C2}$ . III. Electron spin and spin-orbit effects *Phys. Rev.* **147** 295–302
- [32] Cheggour N and Hampshire D P 2002 The unified strain and temperature scaling law for the pinning force density of bronze-route  $\text{Nb}_3\text{Sn}$  wires in high magnetic fields *Cryogenics* **42** 299–309
- [33] Godeke A, Jewell M C, Golubov A A, Ten Haken B and Larbalestier D C 2003 Inconsistencies between extrapolated and actual critical fields in  $\text{Nb}_3\text{Sn}$  wires as demonstrated by direct measurements of  $H_{C2}$ ,  $H^*$  and  $T_c$  *Supercond. Sci. Technol.* **16** 1019–25
- [34] Sekitani T 2004 Upper critical field for optimally-doped  $\text{YBa}_2\text{Cu}_3\text{O}_{7-\delta}$  *Physica B* **346/347** 319–24
- [35] Osofsky M S *et al* 1993 Anomalous temperature dependence of the upper critical magnetic field in Bi-Sr-Cu-O *Phys. Rev. Lett.* **71** 2315
- [36] Zavaritsky V N, Springford M and Alexandrov A S 2000 C-axis negative magnetoresistance and upper critical field of  $\text{Bi}_2\text{Sr}_2\text{CaCu}_2\text{O}_y$  *Europhys. Lett.* **51** 334
- [37] Kaushik S D and Patnaik S 2007 Intergrain connectivity and resistive broadening in vortex state: a comparison between  $\text{MgB}_2$ ,  $\text{NbSe}_2$  and  $\text{Bi}_2\text{Sr}_2\text{Ca}_2\text{Cu}_3\text{O}_{10}$  superconductors *IEEE Trans. Appl. Supercond.* **17** 3016–9
- [38] Clem J 1998 Anisotropy and two-dimensional behaviour in the high-temperature superconductors *Supercond. Sci. Technol.* **11** 909–14
- [39] Lawrence W E and Doniach S 1971 *Proc. 12th Int. Conf. on Low Temperature Physics* ed E Kanda (Kyoto: Academic Press of Japan) p 361
- [40] Hogg M J, Kahlmann F, Barber Z H and Evetts J E 2001 Angular hysteresis in the critical current of  $\text{YBa}_2\text{Cu}_3\text{O}_7$  low-angle grain boundaries *Supercond. Sci. Technol.* **14** 647–50
- [41] Larbalestier D C, Gurevich A, Feldmann D M and Polyanskii A 2001 High- $T_c$  superconducting materials for electric power applications *Nature* **414** 368–77
- [42] Hao Z 1992 Angular dependences of the thermodynamic and electromagnetic properties of the high- $T_c$  superconductors in the mixed state *Phys. Rev. B* **46** 5853–6
- [43] Sneary A B 2000 The fabrication of a high temperature superconducting magnet and critical current characterisation of the component  $\text{Bi}_2\text{Sr}_2\text{Ca}_2\text{Cu}_3\text{O}_x$  tapes and filaments in high magnetic fields *Thesis* Department of Physics, Durham University, pp 1–156
- [44] Tagaya K, Senda K, Yosida T, Fukuoka N and Sasakura H 1992 Lower critical fields in Bi-2212 and Bi-2223 superconductors *Japan. J. Appl. Phys.* **31** L1170–1
- [45] Matsubara I, Tanigawa H, Ogura T, Yamashita H and Kinoshita M 1992 Upper critical field and anisotropy of the high- $T_c$  BSCCO phase *Phys. Rev. B* **45** 7414–7
- [46] Cyrot M and Pavuna D 1992 *Introduction to Superconductivity and High- $T_c$  Materials* (Singapore: World Scientific)
- [47] Martínez J C *et al* 1992 Magnetic anisotropy of a  $\text{Bi}_2\text{Sr}_2\text{CaCu}_2\text{O}_x$  single crystal *Phys. Rev. Lett.* **69** 2276–9
- [48] Taylor D M J and Hampshire D P 2005 The scaling law for the strain dependence of the critical current density in  $\text{Nb}_3\text{Sn}$  superconducting wires *Supercond. Sci. Technol.* **18** S241–52
- [49] Sugano M, Shikimachi K, Hirano N and Nagaya S 2010 The reversible strain effect on critical current over a wide range of temperatures and magnetic fields for YBCO coated conductors *Supercond. Sci. Technol.* **23** 085013
- [50] van der Laan D C 2010 The effect of strain on grain boundaries in  $\text{YBa}_2\text{Cu}_3\text{O}_{7-\delta}$  coated conductors *Supercond. Sci. Technol.* **23** 014004
- [51] van der Laan D C, Haugan T J and Barnes P N 2009 Effect of a compressive uniaxial strain on the critical current density of grain boundaries in superconducting  $\text{YBa}_2\text{Cu}_3\text{O}_7$  films *Phys. Rev. Lett.* **103** 027005
- [52] Welp U *et al* 1992 Effect of uniaxial stress on the superconducting transition in  $\text{YBa}_2\text{Cu}_3\text{O}_7$  *Phys. Rev. Lett.* **69** 2130
- [53] Chen X F, Tessema G X and Skove M J 1991 Effect of elastic stress on the resistivity and  $T_c$  of  $(\text{Bi, Pb})_2\text{Sr}_2\text{Ca}_{n-1}\text{Cu}_n\text{O}_x$  *Physica C* **181** 340–4
- [54] Pugh N, Evetts J and Wallach E 1985 A transmission electron-microscopy study of bronze-processed  $\text{Nb}_3\text{Sn}$  and  $(\text{Nb, Ta})_3\text{Sn}$  multifilamentary superconducting wire *J. Mater. Sci.* **20** 4521–6
- [55] Feldmann D M, Holesinger T G, Feenstra R and Larbalestier D 2008 A review of the influence of grain boundary geometry on the electromagnetic properties of polycrystalline  $\text{YBa}_2\text{Cu}_3\text{O}_{7-x}$  films *J. Am. Ceram. Soc.* **91** 1869
- [56] Ayai N *et al* 2008 Progress in performance of DI-BSCCO family *Physica C* **468** 1747
- [57] Hensel B, Grasso G and Flukiger R 1995 Limits to the critical current in superconducting  $(\text{Bi, Pb})_2\text{Sr}_2\text{Ca}_2\text{Cu}_3\text{O}_{10}$  silver-sheathed tapes: the railway-switch model *Phys. Rev. B* **51** 15456
- [58] Gurevich A and Pashitskii E A 1998 Current transport through low-angle grain boundaries in high-temperature superconductors *Phys. Rev. B* **57** 13878–93

- [59] Goyal A *et al* 1999 Texture formation and grain boundary networks in rolling assisted biaxially textured substrates and in epitaxial YBCO films on such substrates *Micron* **30** 463–78
- [60] Klaassen F C 2001 Vortex pinning by natural linear defects in thin films of  $\text{YBa}_2\text{Cu}_3\text{O}_{7-\delta}$  *Phys. Rev. B* **64** 184523
- [61] Yamasaki H *et al* 1993 Scaling of flux pinning force in epitaxial  $\text{Bi}_2\text{Sr}_2\text{Ca}_2\text{Cu}_3\text{O}_x$  thin films *Phys. Rev. Lett.* **70** 3331–4
- [62] Matsui H *et al* 2012 4-fold enhancement in the critical current density of  $\text{YBa}_2\text{Cu}_3\text{O}_7$  films by practical ion irradiation *Appl. Phys. Lett.* **101** 232601
- [63] Yang P and Lieber C M 1997 Nanostructured high-temperature superconductors: creation of strong-pinning columnar defects in nanorod/superconductor composites *J. Mater. Res.* **12** 2981–96
- [64] Gutierrez J *et al* 2007 Strong isotropic flux pinning in solution-derived  $\text{YBa}_2\text{Cu}_3\text{O}_{7-x}$  nanocomposite superconductor films *Nature Mater.* **6** 367–73
- [65] Selvamanickam V *et al* 2013 Enhanced critical currents in  $(\text{Gd}, \text{Y})\text{Ba}_2\text{Cu}_3\text{O}_x$  superconducting tapes with high levels of Zr addition *Supercond. Sci. Technol.* **26** 035006
- [66] Selvamanickam V *et al* 2012 The low-temperature, high-magnetic-field critical current characteristics of Zr-added  $(\text{Gd}, \text{Y})\text{Ba}_2\text{Cu}_3\text{O}_x$  superconducting tapes *Supercond. Sci. Technol.* **25** 125013
- [67] van der Beek C J *et al* 2002 Strong pinning in high-temperature superconducting films *Phys. Rev. B* **66** 024523
- [68] Dam B *et al* 1999 Origin of high critical currents in  $\text{YBa}_2\text{Cu}_3\text{O}_{7-\delta}$  superconducting thin films *Nature* **399** 439–42
- [69] Aytug T *et al* 2012 Novel tri-modal defect structure in Nb-doped MOCVD  $\text{YBa}_2\text{Cu}_3\text{O}_7$ : a paradigm for pinning landscape control *Supercond. Sci. Technol.* **25** 095013
- [70] Shimojima T *et al* 2011 Orbital-independent superconducting gaps in iron pnictides *Science* **332** 564–7
- [71] Park T *et al* 2008 Isotropic quantum scattering and unconventional superconductivity *Nature* **456** 366–8